Cellulose (2020) 27:8813–8825
https://doi.org/10.1007/s10570-020-03378-1

ORIGINAL RESEARCH

Performance evaluation of hierarchical and conductive fabric-based electrodes decorated with amorphous FeB nanosheets

Baojiang Liu · Baowei Zheng · Yatao Wang · Hongjuan Li · Wei Wang

Received: 1 June 2020 / Accepted: 7 August 2020 / Published online: 19 August 2020
© Springer Nature B.V. 2020

Abstract Flexible electrodes applied in the field of smart wearable products have attracted intense attention. Textile-based electrodes are considered as promising candidate because of their super flexibility and comfort. Recently, amorphous transition metal boride has been introduced in this application. However, the electrochemistry of amorphous FeB has not been systematically studied. To address this problem, the novel amorphous FeB/RGO/cotton flexible electrodes with multidimensional hierarchical structure were firstly prepared with dipping-drying and chemical reduction methods. The preparation methods are simple and cost-effective at room temperature and atmospheric pressure. The concentration of FeB played the key impact on the structure forming process and electrochemical property. Results showed that FeB/RGO/cotton ternary systems exhibited the better specific capacitance than corresponding binary systems. When the scan rate was 5 mV/s, the specific capacitance of these flexible electrodes was up to 203.3 F/g. In addition, these electrodes also exhibited superior cyclic stability and flexibility due to high specific capacitance retention (over 100%). In brief, this paper provides a novel idea for the application of flexible cellulose electrode materials with a novel developing material.

Keywords Amorphous FeB · Textile-based electrodes · RGO · Flexibility · Cyclic stability

B. Liu · Y. Wang · H. Li
Coal Chemical R&D Center of Kailuan Group, Hebei Provincial Technology Innovation Centre of Coal-Based Materials and Chemicals, Tangshan 063018, Hebei Province, China

B. Liu
College of Chemistry, Chemical Engineering & Biotechnology, Donghua University, Shanghai 201620, China

B. Zheng · W. Wang (✉)
Department of Textitle & Garment Engineering, Changshu Institute of Technology, Suzhou 215500, China
e-mail: wangweiwei8660@126.com

Introduction

Wearable and flexible electronic devices have aroused tremendous attention due to their light weight and increasing demand in the field of smart garments, flexible displays and biomonitoring implants (Li et al. 2019a, b; Tebyetekerwa et al. 2019). Therefore, designing and constructing flexible energy supplying device has become the critical route to support the development of wearable electronic devices. Supercapacitors with salient flexibility, high energy density, fast charge-discharge capability, and long-life time are regarded as one of the most promising energy storage devices (Li et al. 2018a; Tseng et al. 2018; Wang et al. 2019a). To prepare high-performance supercapacitors, suitable and flexible electrode with

splendid electrochemical property, lightweight, low-cost and tailorability must be developed.

Many flexible materials include fabrics (Yong et al. 2018; Yun et al. 2015; Yang et al. 2017), fibers (Liu et al. 2015), yarns (Jost et al. 2015), papers (Singu et al. 2017; Yuan et al. 2013) and metal films (Qin et al. 2015) are used as substrates to prepare flexible electrodes. Among these materials, fabrics are considered as the ideal platforms to construct energy storage devices (Lv et al. 2019; Sun et al. 2019). On the one hand, traditional fabrics are of outstanding inherent properties involved hierarchical texture structure, lightweight, super pliability and mechanical strength features. On the other hand, the production cost of textile fabric is low due to its natural abundance. However, the electrically insulated nature of textile fabrics hinder their practical application because of poor electrochemical performance (Sun et al. 2019; Zhao et al. 2017). As conductive agents and double-layer materials, carbon materials are usually used to impart traditional fabrics conductivities and electrochemical properties (Chee et al. 2016; Lima et al. 2018; Xu et al. 2017). Xu and co-workers prepared graphene/cotton fabric electrodes with dipping-drying method (Xu et al. 2015). We also got flexible graphene/fabric electrodes based on cotton fabrics with different texture in our previous report (Wang et al. 2020a). The preparation method is easy and practical. Nevertheless, the low specific capacitances of these flexible electrodes cannot meet high energy storage performance requirements of wearable electronics.

Transition metal compounds have been adopted to compensate for the low energy densities of carbon materials benefited for their pseudo-capacitances. A large number of flexile electrodes integrated with different transition metal compounds are reported to enhance their electrochemical properties (Jeong et al. 2019; Wen et al 2016; Xu et al. 2018; Zhou et al. 2017). Herein, amorphous transition metal borides have been attracting dramatic research interests because of their performances of low-cost, environmental friendly and high pseudo-capacitance (Chen et al. 2017a; Li et al. 2018; Meng et al. 2019; Qin et al. 2018; Wang et al. 2019b, 2020b). Notably, amorphous transition metal borides are often used in the realms of luminescence, electro-catalysis, thermoelectric, oxygen evolution reaction, field emission and magnetic electricity. Recently, their applications have been extended to wearable electronic fields because of the unique structure and characteristics mentioned above (Raula et al. 2012; Wang et al. 2015; Zhou et al. 2012). Chen reported that amorphous Ni-Co-B materials demonstrated the maximum specific capacitance of 2226.96 F/g at a current density of 1 A/g (Chen et al. 2017b). Qin and co-workers created amorphous Ni-B materials with energy density of 137.9 mAh/g (Qin et al. 2018). In our previous report, amorphous Co-Fe-B@RGO@cotton fabric electrodes were developed, and they exhibited a good specific capacitance of 302.6 F/g at the scan rate 5 mV/s (Wang et al. 2020b). All results confirmed that the large surface area and inherent abundant defects of amorphous borides are beneficial for improving the specific capacitance. However, the limited long-term stability of amorphous borides hinder their further development. In addition, only a few reports on amorphous transition borides were issued to study their electrochemical properties. Also there no reports on the supercapacitor application of amorphous FeB material.

Based on the analysis mentioned above, there are two problems should be solved. One is the low capacity of RGO/fabric, resulting from the double-layer property of RGO. While the other are the electrochemical property of amorphous FeB and corresponded long cycle performance, which are not be reported. Advantageous synergistic effects among textile, RGO and amorphous FeB facilitate to improve the electrochemical performance of flexile electrode. Also, adjusting the microstructure of textile-based electrode plays an important effect on the specific capacitance and long-term stability.

Herein, a flexible amorphous FeB/RGO/cotton fabric electrode was firstly prepared by attaching RGO onto the surface of cotton fabric and subsequently loading amorphous FeB nanosheets onto the surface of RGO/cotton fabric. Notably, amorphous FeB was successfully prepared at room temperature, along with a short time of 10 min. These simple and mild conditions avoid the damage to mechanical properties of textile fabric caused by heat treatment or hazardous solvent. Also the effect of Fe^{3+} concentration on the forming structure of textile-based electrode was studied. In addition, the bending times and bending angles on the electrochemical performance of FeB/RGO/cotton electrode were also systematically evaluated. Results showed that this fabric electrode exhibited a high specific capacitance of 203.3 F/g at

the scan rate of 5 mV/s. In addition, FeB/RGO/cotton composite electrode displayed an outstanding flexibility and cycling stability, with over 100% retention of the initial specific capacitance.

Experimental procedure

Materials and regents

Ferric chloride hexahydrate ($FeCl_3{\cdot}6H_2O$), sodium borohydride ($NaBH_4$), sodium hydroxide (NaOH) and sodium sulfate (Na_2SO_4) were obtained from Sinopharm Chemical Reagent Co., Ltd. All reagents with AR grade were used without any additional processing. Graphene oxide (GO) was provided by Beijing Boyu Co., Ltd. Woven cotton fabric was purchased from Shaoxing Aobang Textile Company.

Preparation of FeB/RGO/cotton fabric electrodes

Firstly, RGO sheets were deposited on the surface of cotton fabric with conventional dipping-drying method (Xu et al. 2015). 1 g of GO powders was added into 500 ml of double-deionized water and dispersed evenly with ultrasonic apparatus for 30 min. Then cotton fabric rinsed with NaOH aqueous solution (1 mol/L) was added into it. After being immersed for 30 min, cotton fabric was taken out and dried at 60 °C for 2 h. The above process was repeated for ten times. $NaBH_4$ with the concentration of 0.6 mol/L was used to reduce GO to conductive RGO. Secondly, four $FeCl_3{\cdot}6H_2O$ solutions with different concentration of 0.18 mol/L, 0.12 mol/L, 0.09 mol/L and 0.06 mol/L were configured, respectively, and labelled as solution A. Subsequently, RGO/cotton fabric with size of 1*2 cm^2 was put into solution A for 30 min. At the same time, 5 mmol NaOH and 25 mmol $NaBH_4$ were added into 20 mL deionized water to form solution B, and added dropwise to the solution A. After reacted for 10 min, the treated cotton fabric was taken out and washed thoroughly, finally dried at 60 °C to obtain FeB/RGO/cotton sample. The simplified process for the synthesis of FeB/RGO/cotton is described in Fig. 1.

Characterization

Scanning electron microscopy (SEM, SU8010, Hitachi) and transmission electron microscope (TEM, JEM-2100) were used to observe the surface morphology of textile electrode. Elemental mapping and energy dispersive spectrometer (SEM-EDS) were employed to confirm the elemental distribution. Selected area electron diffraction (SAED) patterns from HR-TEM measurement were measured to analyze the crystalline structure of FeB. X-ray diffractometer (XRD) was adopted to detect the crystal structures of textile electrodes. Element compositions and chemical bonding states of textile electrodes were measured with X-ray photoelectron spectrometry (XPS, Thermo Scientific Escalab, USA). The surface sheet conductivity of this fabric electrode was measured through four-point probe tester of RTS-8. Cyclic voltammogram curve (CV), galvanostatic charge/discharge curve (GCD) and electrochemical impedance spectra (EIS) were characterized with three-electrode configuration using CHI660E Instruments (Chenhua Instruments Corporation, Shanghai). In detail, 1 mol/L of Na_2SO_4 was used as electrolyte. Pt foil, Ag/AgCl electrode and fabric electrode with size of 1 cm*1 cm were adopted as counter electrode, reference electrode and working electrode, respectively. Specific capacitance was calculated based on the CV curves with the equation as followed.

$$C = \frac{1}{sm\Delta V}\int_{v0}^{v0+\Delta V} idV \tag{1}$$

where C is the specific capacitance; s is the scan rate, m is the active material mass; ΔV is the voltage window.

Results and discussion

Structure of amorphous FeB/RGO/cotton fabric electrodes

Surface morphologies of original cotton fabric, RGO/cotton and FeB/RGO/cotton fabric electrode were observed with SEM measurement. From Fig. 2a, the surface of pure cotton fabric composed of naturally twisted fiber bundles was smooth. After the

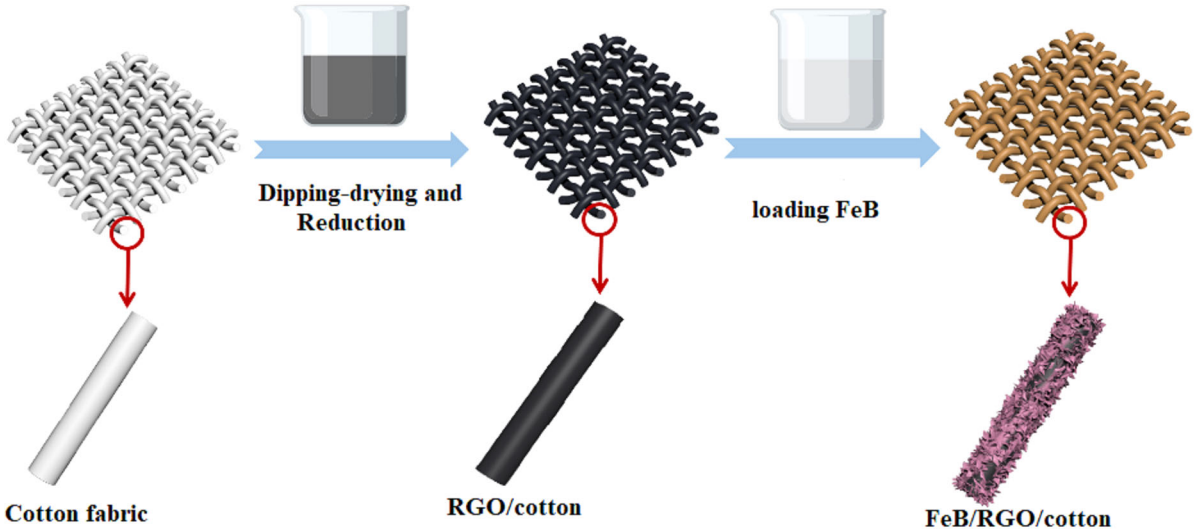

Fig.1 Schematic diagram of amorphous FeB/RGO/cotton electrode

introduction of RGO, cotton fabric surface was coated by RGO sheets with several micrometers, as shown in Fig. 2 (b). SEM images of FeB/RGO/cotton fabric composite (Fe^{3+} concentration was 0.12 mol/L) were depicted in Fig. 2(c and d). Clearly, each fiber bundle of this flexible electrode was wrapped with FeB flakes. From SEM images with high magnification of Fig. 2 (d), it was clear that a large number of nanoscale flakes attached on the RGO/cotton fabric surface, along with good compatibility and tight integration between RGO and FeB. Herein, the effect of Fe^{3+} concentration on the structure forming was studied in depth. According to SEM images in Fig. 3, all other three FeB/RGO/cotton fabric composites exhibited granular structure, no matter the concentration of Fe^{3+} was 0.18 mol/L, 0.09 mol/L or 0.06 mol/L. When the concentration was low to 0.06 mol/L (Fig. 3a, b), most particles were spherical, and aggregated seriously. Increased the concentration to 0.09 mol/L (Fig. 3c, d), the particles with decreased size had become irregular. But these particles also aggregated seriously. When the concentration was up to 0.18 mol/L, a portion of these particles aggregated into larger particles attaching on the fabric surface. Only the composite electrodes prepared with 0.12 mol/L of Fe^{3+} showed the relatively and uniformly distributed flake structure, which were beneficial for exposing to electrolyte and shorten the distance of ion diffusion transportation. Because the electrochemical performances of these electrodes are directly related to their microscopic appearance. Therefore, the concentration of Fe^{3+} is a key factor to affect the electrode performance. The relationship between Fe^{3+} concentration and performance of this electrode was discussed in detail below.

The element composition and distribution of the as-made fabric composites were detected, and results were shown in Fig. 2(e and f). Four elements C, O, B and Fe were all found on the fabric surface. The large amount of C and O originated from carbon-containing functional groups of cotton fibers and RGO, while B and Fe with the atom percent ratio 1:3 were attributed to FeB flakes. The results of EDS and Mapping test confirmed that RGO and FeB were both successfully coated on the fabric surface, which was helpful for improving electrochemical performance.

Furthermore, microstructures of FeB and RGO on the surface of cotton fabric were detected with TEM measurement. Before the test, FeB/RGO/cotton fabric was ultrasonic for 60 min to ensure FeB and RGO fall off from the surface of cotton fabric. From Fig. 4a, b, FeB and RGO were easily observed, confirming that they both well anchored on cotton surface. No obvious crystal lattice of FeB was detected, suggesting its typical amorphous structure, as shown in Fig. 4c. This result was also confirmed with SAED test in Fig. 4d because of a broad and diffused halo ring. As the previously reported in the literature, it was because that essential defects or vacancies and long-range atomic arrangement disorder determined the

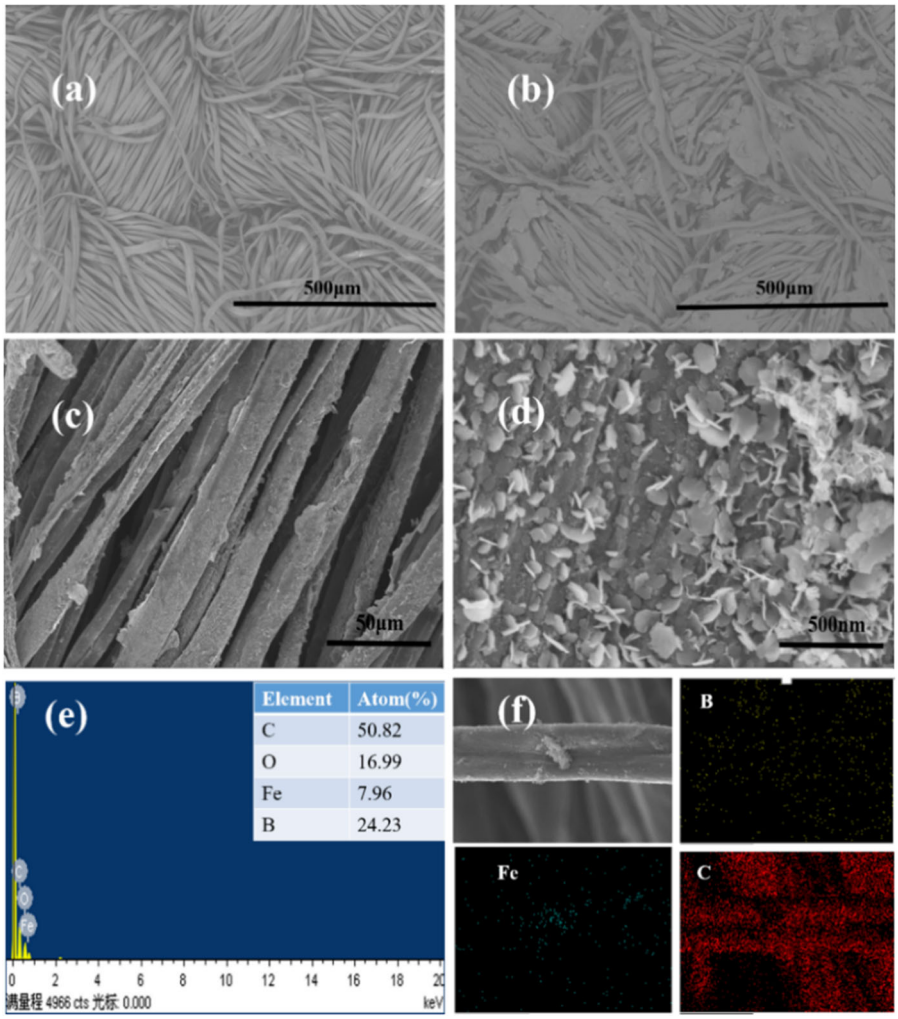

Fig. 2 SEM images: **a** Cotton; **b** RGO/cotton; **c**, **d** FeB/RGO/cotton fabric; **e** EDS analysis of FeB/RGO/cotton fabric sample, **f** Mapping image of FeB/RGO/cotton fabric sample. Note: Fe^{3+} concentration was 0.12 mol/L

electrochemical performance of amorphous materials (Li et al. 2018b; Meng et al. 2019).

X-ray diffraction technology was adopted to analyze crystal structure and phase composition of this fabric electrode. As shown in Fig. 5a, all diffraction peaks of cotton fabric at 2θ = 14.36°,16.36°, 22.60° and 33.98° corresponded to cellulose I. The peaks observed in RGO/cotton fabric and FeB/RGO/cotton fabric electrode were same with those of original cotton fabric because of the relative low amount of RGO and FeB. The formation mechanism of FeB was speculated as followed:

$$BH_4^- + 2Fe^{3+} \leftrightarrow BO_2^- + 2Fe + 2H_2 + 6H^+ \quad (2)$$

$$BH_4^- + 3H_2O \leftrightarrow B + OH^- + 2.5H_2 \quad (3)$$

XPS measurement was employed to verify the chemical composition and chemical state of the composite cotton fabric electrode. Clearly, Fe, B, O and C were all seen in the sample of FeB/RGO/cotton fabric composite from Fig. 5b, which was consistent with EDS result. From the high-resolution of Fe 2p spectra in Fig. 5c, it was clear that Fe 2p has two characteristic peaks located at 711.8 eV and 725.1 eV, which were ascribed to Fe 2p3/2 and Fe 2p1/2, respectively. Satellite peaks of Fe2p spectrum centered at 719.1 eV and 733.3 eV were also found,

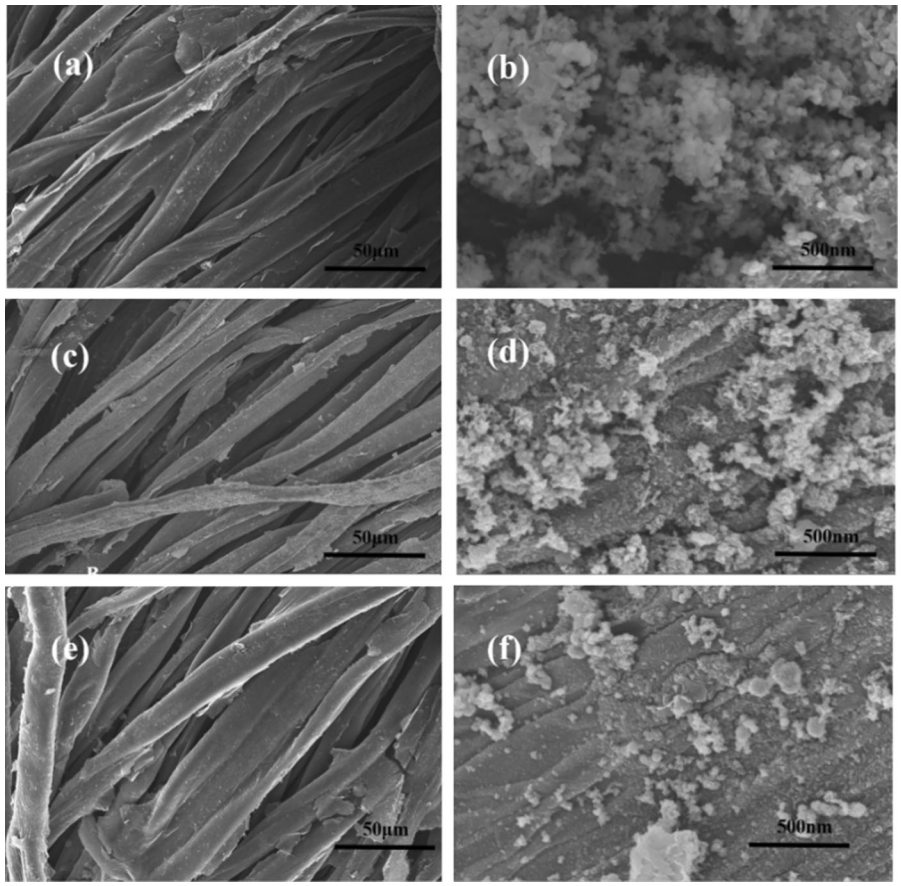

Fig.3 SEM images of FeB/RGO/cotton fabric with different Fe^{3+} concentration: **a**, **b** 0.06 mol/L; **c**, **d** 0.09 mol/L; **e**, **f** 0.18 mol/L

suggesting that Fe was in the elemental and oxidized states (Meng et al. 2019). Only one peak at 192.17 eV was deconvoluted in the B1s spectrum of FeB/RGO/fabric composite electrode, showing that boron was in oxidized state (Meng et al. 2019). The chemical states of Fe and B were consistent with the theoretical results of amorphous FeB alloy. From Fig. 5e, c spectrum displayed four peaks at 284.7 eV, 286.7 eV, 288.4 eV and 289.3 eV attributing to C-C, C-O, C=O and O-C=O, respectively. In addition, three peaks at 530.18 eV, 531.74 eV and 533.08 eV were found in XPS spectra of O1s, as shown in Fig. 5f. The binding energy at 530.18 eV was ascribed as O-M because of the surface phases of FeO. Binding energy of O 1 s at 531.74 eV presented for absorbed O_2, while that of O1s at 533.08 eV corresponded OH caused by absorbed H_2O (Meng et al. 2019; Chen et al. 2017b; Kong et al. 2018).

Electrochemical property of amorphous Fe-B/RGO/cotton fabric electrode

To verify the synergy effect of RGO and amorphous FeB alloy on the electrochemical property, CV curves of FeB/cotton composite electrode, RGO/cotton composite electrode and FeB/RGO/cotton composite electrode were measured, and results were shown in Fig. 6a. Clearly, FeB/RGO/fabric ternary electrode exhibited a much larger CV curve area than FeB/fabric and RGO/fabric, suggesting the best electrochemical character. The low capacity of RGO/cotton was due to the typical double-layer property of RGO. While the low electrochemical performance of FeB/cotton electrode resulted from the non-conductivity of cotton fabric, which was consistent with the electrical conductivity results. The sheet resistances of cotton fabric and FeB@cotton fabric were not be detected, while those of RGO/fabric and FeB/RGO/fabric were

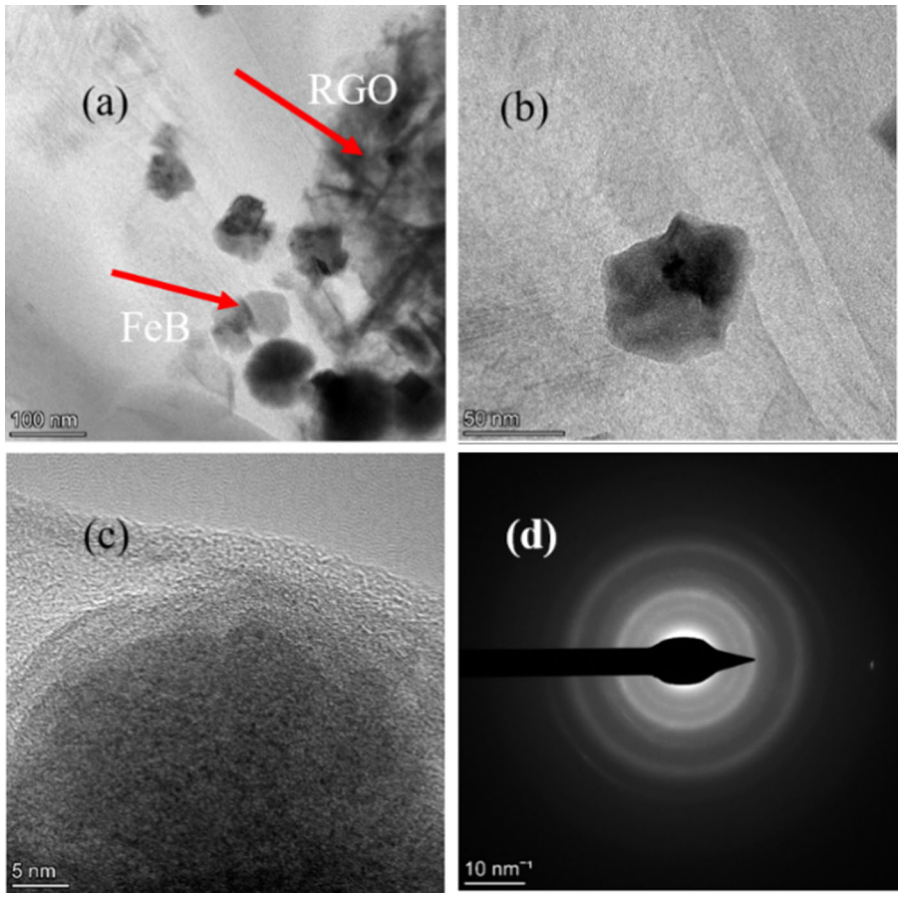

Fig.4 TEM images of FeB/RGO/fabric **a**, **b** TEM images, **c** HRTEM Image, **d** SAED pattern

206Ω/sq and 173Ω/sq, respectively. In other words, superb synergistic effect between RGO and FeB promoted the electrochemical performance of FeB/RGO/cotton composites. The high conductivity of RGO greatly improved charge carriers mobility, while amorphous Fe-B remarkably enhanced the specific capacitance.

The effect of Fe^{3+} concentration on electrochemical property of FeB/RGO/cotton fabric electrodes was studied with three-electrode configuration system. From Fig. 6b, all FeB/RGO/cotton electrodes had the approximately symmetric CV curves. The as-made sample with Fe^{3+} concentration of 0.12 mol/L showed the largest closure area of CV curve among these four composite electrodes. As for other three samples with different Fe^{3+} concentration, the closure area of FeB/RGO/cotton with Fe^{3+} concentration of 0.09 mol/L was a little bigger than that with Fe^{3+} concentration of 0.06 mol/L. While the closure area of FeB/RGO/cotton with Fe^{3+} concentration of 0.18 mol/L was smallest. These results showed the specific capacitance of FeB/RGO/cotton with Fe^{3+} concentration of 0.12 mol/L was optimum among these four samples. Also, FeB/RGO/cotton electrode with Fe^{3+} concentration of 0.12 mol/L exhibited a longest charge–discharge time in Fig. 6c. The charge–discharge time of FeB/RGO/cotton electrode with Fe^{3+} concentration of 0.09 mol/L was longer, while that of FeB/RGO/cotton electrode with Fe^{3+} concentration of 0.18 mol/L was shortest. The change trend was the same with the CV results. All these conclusions confirmed that FeB/RGO/cotton fabric electrode with Fe^{3+} concentration of 0.12 mol/L exhibited the best capacitive behavior and highest coulomb efficiency. Maybe that the uniformly distributed sheet structure of FeB/RGO/cotton fabric electrodes was favorable for exposing to electrolyte and providing a high-speed pathway for ionic transportation to proceed

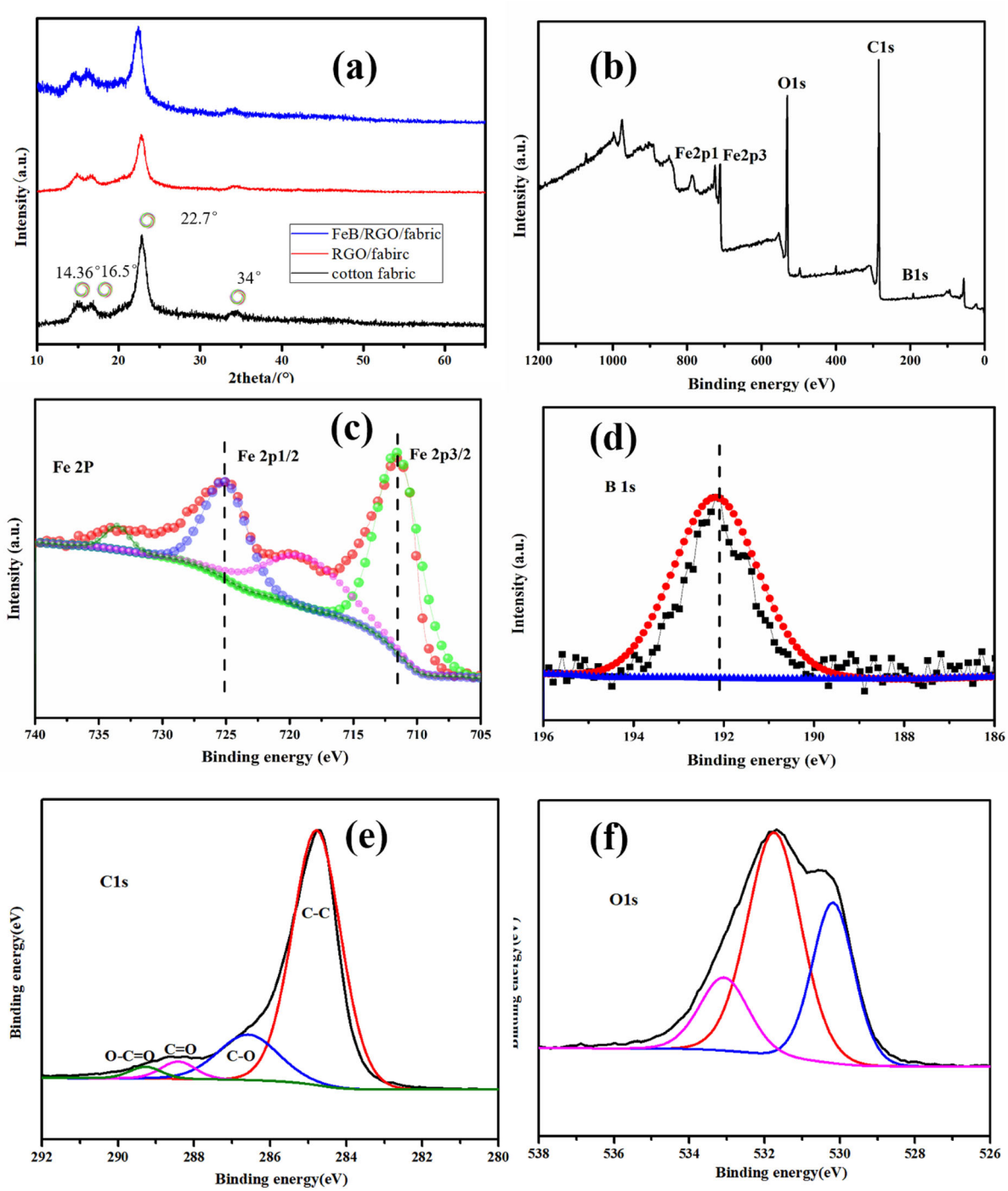

Fig. 5 **a** XRD of cotton, RGO/cotton and FeB/RGO/cotton fabric; **b** XPS survey spectra of FeB/RGO/cotton fabric; **c** high resolution XPS spectrum of Fe 2p; **d** high resolution XPS spectrum of B 1s. **e** High resolution XPS spectrum of C 1s; **f** high resolution XPS spectrum of O 1s

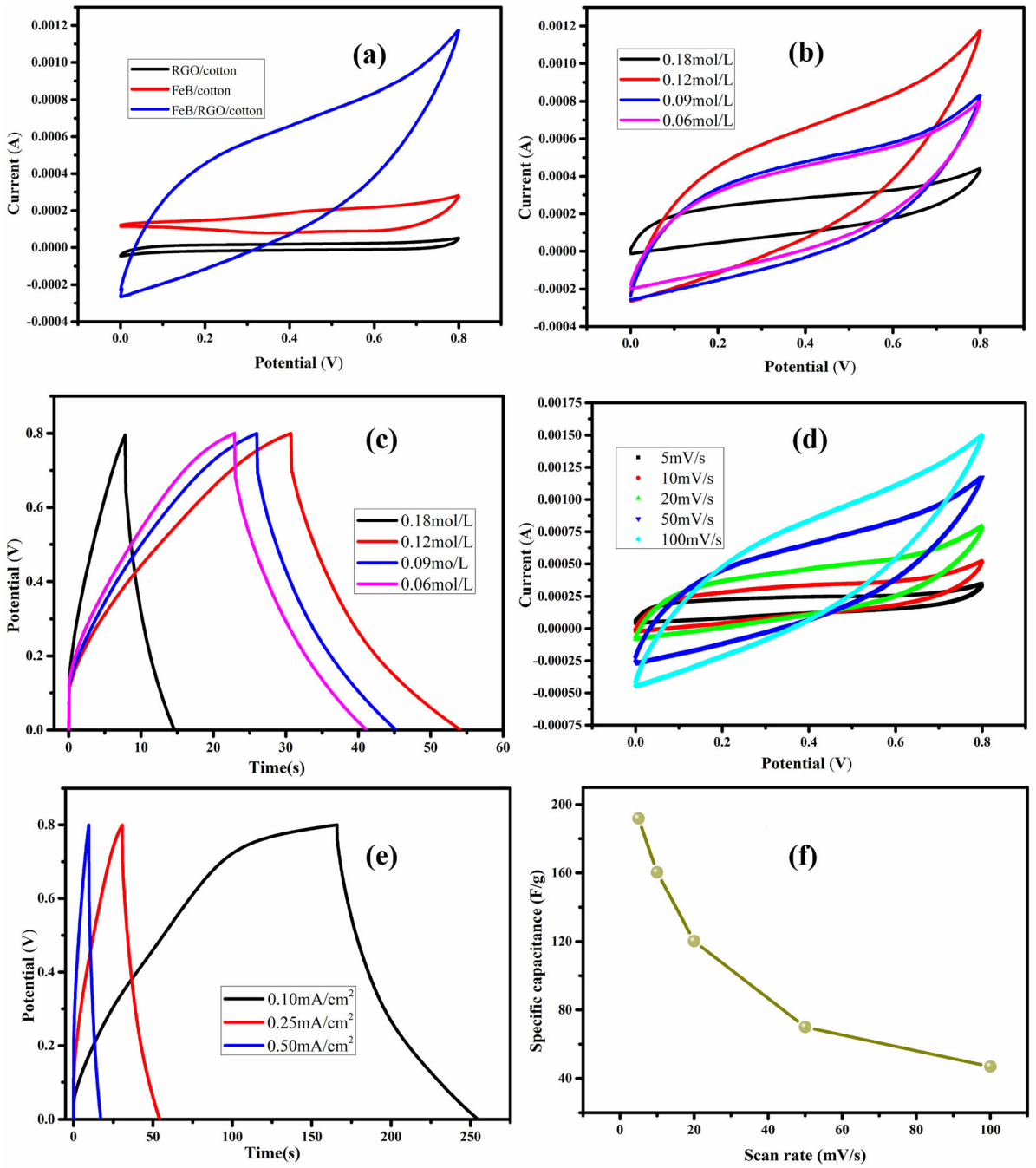

Fig. 6 **a** CV curves of RGO/cotton, FeB/cotton and FeB/RGO/cotton electrodes at the scan rate of 50 mV/s; **b** CV curves of FeB/RGO/cotton electrodes with different Fe^{3+} concentration at the scan rate of 50 mV/s; **c** GCD curves of FeB/RGO/cotton electrodes with different Fe^{3+} concentration under current density of 0.25 mA/cm^2; **d** CV curves of FeB/RGO/cotton electrodes with Fe^{3+} concentration of 0.12 mol/L at the different scan rate; (e) GCD curves of FeB/RGO/cotton electrodes with Fe^{3+} concentration of 0.12 mol/L with different current densities; **f** the relationship between scan rate and specific capacitance

electrochemical reaction. And other three samples were all composed of aggregate nanoparticles with different sizes, which reduced the expose extent to the electrolyte and limited the transportation of charge carriers.

Based on the results mentioned above, CV curves of the optimum FeB/RGO/cotton fabric electrode with Fe^{3+} concentration of 0.12 mol/L at different scan rates from 5 mV/s to 100 mV/s were detected. As shown in Fig. 6d, all CV curves exhibited almost rectangular shape, demonstrating the superior electrochemical behavior. The closure area of CV curve increased with the increase of the scan rate, which meeted the standard of flexible electrodes. The specific capacitance calculated according to CV curves were about 203.3F/g, 192.5F/g, 144.4F/g, 84F/g and 56.3F/g corresponded to the scan rate of 5 mV/s, 10 mV/s, 20 mV/s, 50 mV/s and 100 mV/s, respectively (Fig. 6f). GCD curves of optimum FeB/RGO/cotton electrodes with different current densities were also tested in Fig. 6e.Clearly, the composite fabric electrode gave the similar curve shapes at current densities of 0.5 mA/cm^2, 0.25 mA/cm^2 and 0.10 mA/cm^2. Notably, there is no obvious pressure drop on the GCD curves, indicating an ideal capacitor behavior.

EIS measurement was conducted to further clarify the energy storage mechanism of FeB/RGO/cotton electrodes, and the result was described in Fig. 7a. From the inset image corresponded to equivalent circuit, the intersection point between the real axis and high frequency part in Nyquist curve represents the equivalent series resistance Rs, which results from the resistance between the internal electrode and electrolyte system. The resistance between the electrode and electrolyte interface stands for the charge transfer resistance Rct, which comes from the partial semicircle. The Warburg diffusion process (W) depicted by the linear line of the low frequency, which is used to verify the ion diffusion transport. The constant elements are attributed to the double layer capacitance property (CPE1) and pseudo capacitance property (CPE2). Clearly, Rct and W of FeB/RGO/cotton electrode were relatively small, indicating the weak electrochemical resistance. Maybe the evenly distributed ultrathin lamellar structure contributed to the electron transfer between the as-made samples and electrolyte.

Figure 7b showed the long-term cycling electrochemical performance of FeB/RGO/cotton electrodes at the current density of 0.5 mA/cm^2 for 3000 charge-discharge cycles. The specific capacitance increased with increasing cycling number due to the activation process. After 3000 cycles, the specific capacitance increased to 120.9% of original capacitance, which indicated an excellent stability. The reason maybe explained as followed. During initial charge-discharge process, only a small fraction of FeB material was activated to participate the reaction (Meng et al. 2019). Increased cycle numbers, more and more interior parts of the active materials could be activated and interacted with electrolyte ions to improve the electrochemical performance. Therefore, a higher specific capacitance was obtained when the cycle numbers increased. (Nagaraju et al. 2017; Wang et al. 2017).

In addition, the flexibility of FeB/RGO/cotton fabric electrodes was also evaluated with different bending numbers and bending angles. From Fig. 7(c), it was clear that CV curves of FeB/RGO/cotton fabric electrodes overlapped. Even being bended for 400 times, there was no obvious change on the CV curve. And the capacitance retention was up to 100.1% compared with the original sample, indicating its splendid flexibility. The capacitances of FeB/RGO/cotton electrodes with different bending angles were also studied to confirm their super stability. The composite fabric electrodes also showed excellent flexible properties for the overlapped CV curves with different bending angles, as shown in Fig. 7e. Notably, the capacitances of FeB/RGO/cotton electrodes increased with the increasing of bending angles. When the bending angle was 180°, the specific capacitance increased to 103% of original capacitance, as depicted in Fig. 7f. Maybe the active material was activated in the bending process, promoting the interaction between the active materials and electrolyte ions. The results mentioned above suggested a superior excellent flexibility performance of these fabric electrodes.

Conclusion

In summary, a novel FeB/RGO/cotton composite electrode system was successfully prepared by the facile dipping-drying and chemical reduction method. Amorphous FeB nanosheets attached on the surface of RGO/cotton fabric electrodes were beneficial for the

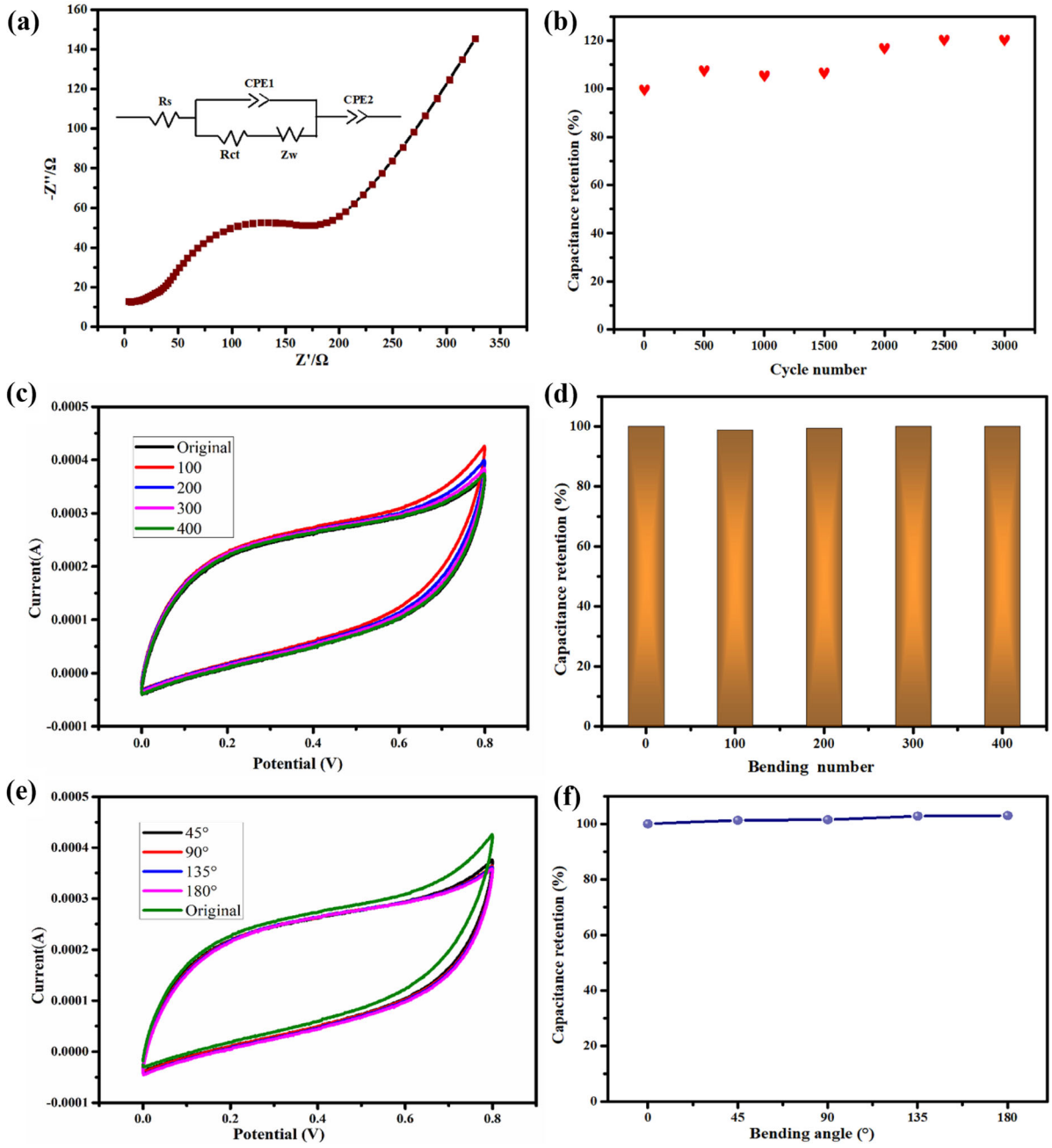

Fig. 7 **a** Electrochemical inductance spectra of FeB/RGO/cotton fabric electrode; **b** Cycling performance at a current density of 0.25 mA/cm^2; **c** CV curves of FeB/RGO/cotton fabric electrode with different bended times; **d** Specific capacitance retention with different bended times; **e** CV curves of FeB/RGO/cotton fabric electrode with different bended angle; **d** Specific capacitance retention with different bended angle

enhanced electrochemical property. When Fe^{3+} concentration was 0.12 mol/L, FeB/RGO/cotton composite electrodes exhibited optimum capacitance of 203.3 F/g at the scan rate of 5 mV/s, resulting from the uniformly distributed nanosheets. In addition, the improved capacities of these fabric electrodes were also ascribed to the synergistic effect of conductivity, shorten ion transfer paths, more accessible

electroactive sites and high electron collection efficiency. Moreover, the composite cotton fabric electrodes showed an outstanding cycle stability and flexibility, since that the specific capacitances of these amorphous FeB/RGO/cotton composite electrodes after being bended for 400 cycles or different bended angles can still be maintained over 100%. In summary, this paper provides a novel idea for the application of flexible cellulose electrode materials with a simple and low-cost method.

Acknowledgments The authors are grateful for the financial support of this research by "Natural Science Foundation of Jiangsu Province" (No.BK20181038)

References

Chee WK, Lim HN, Zainal Z, Huang NM, Harrison I, Andou Y (2016) Flexible graphene-based supercapacitors: a review. J Phys Chem C 120:4153–4172. https://doi.org/10.1021/acs.jpcc.5b10187

Chen RN, Liu L, Zhou JS, Hou L, Gao FM (2017a) High-performance nickel-cobalt-boron material for an asymmetric supercapacitor with an ultrahigh energy density. J Power Sources 341:75–82. https://doi.org/10.1016/j.jpowsour.201611.108

Chen HY, Ouyang SX, Zhao M, Li YX, Ye JH (2017b) Synergistic activity of Co and Fe in amorphous Cox-Fe-B catalyst for efficient oxygen evolution reaction. ACS Appl Mater Interfaces 9:40333–40343. https://doi.org/10.1021/acsami.7b13939

Jeong YM, Son I, Baeka SH (2019) Binder-free of NiCo-layered double hydroxides on Ni-coated textile for wearable and flexible supercapacitors. Appl Surf Sci. 467–468:963–967. https://doi.org/10.1016/j.apsusc.2018.10.252

Jost K, Durkin DP, Haverhals LM, Brown EK, Langenstein M, Long DHC, Trulove PC, Gogotsi Y, Dion G (2015) Natural fiber welded electrode yarns for knittable textile supercapacitors. Adv Energy Mater 5:1401286. https://doi.org/10.1002/aenm.201401286

Kong XC, Xu YM, Cui ZD, Li ZY, Liang YQ, Gao ZH, Zhu SL, Yang XJ (2018) Defect enhances photocatalytic activity of ultrathin TiO_2 (B) nanosheets for hydrogen production by plasma engraving method. Appl Catal B Environ 230:11–17. https://doi.org/10.1016/j.apcatb.2018.02.019

Li X, Liu R, Xu C, Bai Y, Zhou X, Wang Y, Yuan G (2018a) High-performance polypyrrole /graphene/$SnCl_2$ modified polyester textile electrodes and yarn electrodes for wearable energy storage. Adv Funct Mater 28:1800064. https://doi.org/10.1002/adfm.201800064

Li Q, Xu YX, Zheng SS, Guo XT, Xue HG, Pang H (2018b) Recent progress in some amorphous materials for supercapacitors. Small. https://doi.org/10.1002/smll.201800426

Li YZ, Zhang YF, Zhang HR, Xing TL, Chen GQ (2019a) A facile approach to prepare a flexible sandwich structured supercapacitor with rGO-coated cotton fabric as electrodes. RSC Adv 9:180–4189. https://doi.org/10.1039/C9RA00171A

Li ZQ, Tian MW, Sun XT, Zhao HT, Zhu SF, Zhang XS (2019b) Flexible all-solid planar fibrous cellulose nonwoven fabric-based supercapacitor via capillarity-assisted graphene/MnO_2 assembly. J Alloys Compd 782:986–994. https://doi.org/10.1016/j.jallcom.2018.12.254

Lima RMAP, Alcarazespinoza JJ, Silva FAGD, Oliveira HPD (2018) Multifunctional wearable electronic textiles using cotton fibers with polypyrrole and carbon nanotubes. ACS Appl Mater Inter 10:13783–13795. https://doi.org/10.1021/acsami.8b04695

Liu LB, Yu Y, Yan C, Li K, Zheng ZJ (2015) Wearable energy-dense and power-dense supercapacitor yarns enabled by scalable graphene-metallic textile composite electrodes. Nat Commun 6:7260. https://doi.org/10.1038/ncomms8260

Lv JC, Zhang LP, Zhong Y, Sui XF, Wang BJ, Chen ZZ, Feng XL, Xu H, Mao ZP (2019) High-performance polypyrrole coated knitted cotton fabric electrodes for wearable energy storage. Org Electron 74:59–68. https://doi.org/10.1016/j.orgel.2019.06.027

Meng QZ, Xu W, Zhu SL, Liang YQ, Cui ZD, Yang XJ, Inoue A (2019) Low-cost fabrication of amorphous cobalt-iron-boron nanosheets for high-performance asymmetric supercapacitors. Electrochim Acta 296:198–205. https://doi.org/10.1016/j.electacta.2018.11.067

Nagaraju G, Cha SM, Sekhar SC, Yu JS (2017) Metallic layered polyester fabric enabled nickel selenide nanostructures as highly conductive and binderless electrode with superior energy storage performance. Adv Energy Mater 7:1601362. https://doi.org/10.1002/aenm.201601362

Qin KQ, Kang JL, Li JJ, Shi CS, Li YX, Qiao ZJ, Zhao NQ (2015) Free-Standing porous carbon nanofiber/ultrathin graphite hybrid for flexible solid-state supercapacitors. ACS Nano 9:481–487. https://doi.org/10.1021/nn505658u

Qin W, Liu Y, Liu XY, Yang GW (2018) Facile scalable production of amorphous nickel borate for high performance hybrid supercapacitors. J Mater Chem. 40:19689–19695. https://doi.org/10.1039/C8TA07385F

Raula M, Rashid MH, Lai S, Roy M, Mandal TK (2012) Solventadoptable polymer Ni/NiCo alloy nanochains: highly active and versatile catalysts for various organic reactions in both aqueous and nonaqueous media. ACS Appl Mater Inter 4:878–889. https://doi.org/10.1021/am201549a

Singu DC, Joseph B, Velmurugan V, Ravuri S, Grace AN (2017) Combustion synthesis of graphene from waste paper for high performance supercapacitor electrodes. Int J N 17:1760023. https://doi.org/10.1142/S0219581X17600237

Sun C, Li X, Cai ZS, Ge FY (2019) Carbonized cotton fabric in-situ electrodeposition polypyrrole as high-performance flexible electrode for wearable supercapacitor. Electrochim Acta 296:617–626. https://doi.org/10.1016/j.electacta.2018.11.045

Tebyetekerwa M, Marriam I, Xu Z, Yang SY, Zhang H, Zabihi F, Jose RJ, Peng SJ, Zhu MF, Ramakrishna S (2019) Critical insight: challenges and requirements of fiber electrodes for wearable electrochemical energy storage. Energy Environ Sci 12:2148–2160. https://doi.org/10.1039/C8EE02607F

Tseng L, Hsiao C, Nguyen DD, Hsieh P, Lee C, Tai N (2018) Activated carbon sandwiched manganese dioxide/graphene ternary composites for supercapacitor electrodes. Electrochim Acta 266:284–292. https://doi.org/10.1016/j.electacta.2018.02.029

Wang H, Ma Y, Wang R, Key J, Linkovb V, Ji S (2015) Liquid-liquid interface-mediated room-temperature synthesis of amorphous NiCo pompoms fromultrathin nanosheets with high catalytic activity for hydrazine oxidation. Chem Commun 51:3570–3573. https://doi.org/10.1039/C4CC09928A

Wang Y, Lai WH, Wang N, Jiang Z, Wang XY, Zou PC, Lin ZY, Fan HJ, Kang FY, Wong CP, Yang C (2017) A reduced graphene oxide/mixed-valence manganese oxide composite electrode for tailorable and surface mountable supercapacitors with high capacitance and super-long life. Energy Environ Sci 10:941–949. https://doi.org/10.1039/c6ee03773a

Wang YJ, Li XL, Wang YM, Liu Y, Bai Y, Liu R, Yuan GH (2019a) High-performance flexible MnO_2@carbonized cotton textile electrodes for enlarged operating potential window symmetrical supercapacitors. Electrochimi Acta 299:12–18. https://doi.org/10.1016/j.electacta.2-018.12.181

Wang S, He P, Xie ZW, Jia LP, He MQ, Zhang XQ, Dong FQ, Liu HH, Zhang Y, Li CX (2019b) Tunable nanocotton-like amorphous ternary Ni-Co-B: a highly efficient catalyst for enhanced oxygen evolution reaction. Electrochim Acta 296:644–652. https://doi.org/10.1016/j.electacta.2018.11.099

Wang W, Li T, Liu K, Wang S, Peng HX (2020a) Effects of three fabric weave textures on the electrochemical and electrical properties of reduced graphene/textile flexible electrodes. RSC Adv 10:6249. https://doi.org/10.1039/c9ra08524f

Wang W, Li T, Sun YY, Liu LG, Wu JB, Yang G, Liu BJ (2020b) Facile and mild method to fabricate a flexible cellulose-based electrode with reduced graphene and amorphous cobalt-iron-boron alloy for wearable electronics. Cellulose 27:7079–7092. https://doi.org/10.1007/s10570-020-03269-5

Wen P, Fan M, Yang D, Wang Y, Cheng H, Wang J (2016) An asymmetric supercapacitor with ultrahigh energy density based on nickle cobalt sulfide nanocluster anchoring multiwall carbon nanotubes hybrid. J Power Sources 320:28–36. https://doi.org/10.1016/j.jpowsour.2016.04.066

Xu LL, Guo MX, Liu S, Bian SW (2015) Graphene/cotton composite fabrics as flexible electrode materials for electrochemical capacitors. RSC Adv 5:25244–25249. https://doi.org/10.1039/C4RA16063K

Xu LS, Jia MY, Li Y, Zhang SF, Jin XJ (2017) Design and synthesis of graphene/activated carbon/polypyrrole flexible supercapacitor electrodes. RSC Adv 7:31342–31351. https://doi.org/10.1039/C7RA04566B

Xu GH, Zhang Z, Qia X, Ren XH, Liu SH, Chen Q, Huang ZY, Zhong JX (2018) Hydrothermally synthesized $FeCo_2O_4$ nanostructures: Structural manipulation for high-performance all solid-state supercapacitors. Ceram Int 44:120–127. https://doi.org/10.1016/j.ceramint.2017.09.146

Yang Y, Huang QY, Niu LY, Wang DR, Yan C, She YY, Zheng ZJ (2017) Waterproof, ultrahigh areal-capacitance, wearable supercapacitor fabrics. Adv Mater 29:1606679. https://doi.org/10.1002/adma.201606679

Yong S, Owen J, Beeby S (2018) Solid-state supercapacitor fabricated in a single woven textile layer for E-textiles applications Adv Eng Mater 20:1700860. https://doi.org/10.1002/adem.201700860

Yuan L, Yao B, Hu B, Huo K, Chen W, Zhou J (2013) Polypyrrole-coated paper for flexible solid-state energy storage. Energ Environ Sci 6:470–476 https:// doi.org/10.1039/c2ee23977a.

Yun TG, Hwang BI, Kim D, Hyun S, Han SM (2015) Polypyrrole-MnO_2-Coated textile-based flexible-stretchable supercapacitor with high electrochemical and mechanical reliability. ACS Appl Mater Inter 7:9228–9234. https://doi.org/10.1021/acsami.5b01745

Zhao J, Li X, Li XY, Cai ZS, Ge FY (2017) A flexible carbon electrode based on traditional cotton woven fabrics with excellent capacitance. J Mater Sci 52(2017):9773–9779. https://doi.org/10.1007/s10853-017-1161-z

Zhou S, Wen M, Wang N, Wu Q, Cheng L (2012) Highly active NiCo alloy hexagonal nanoplates with crystal plane selective dehydrogenation and visible-light photocatalysis. J Mater Chem 22:16858–16864. https://doi.org/10.1039/C2JM32397D

Zhou R, Han CJ, Wang XM (2017) Hierarchical MoS_2-coated three-dimensional graphene network for enhanced supercapacitor performances. J Power Sources 352:99–110. https://doi.org/10.1016/j.jpowsour.2017.03.134

Publisher's Note Springer Nature remains neutral with regard to jurisdictional claims in published maps and institutional affiliations.